Received 8 March 2021
Revised 6 September 2021
Accepted 26 October 2021

Bayesian inference of multi-sensors impedance cardiography for detection of aortic dissection

Vahid Badeli
Institute of Fundamentals and Theory of Electrical Engineering, Graz University of Technology, Graz, Austria

Sascha Ranftl
Institute of Theoretical and Computational Physics, Graz University of Technology, Graz, Austria

Gian Marco Melito
Institute of Mechanics, Graz University of Technology, Graz, Austria

Alice Reinbacher-Köstinger
Institute of Fundamentals and Theory in Electrical Engineering, Graz University of Technology, Graz, Austria

Wolfgang Von Der Linden
Institute of Theoretical and Computational Physics, Graz University of Technology, Graz, Austria

Katrin Ellermann
Institute of Mechanics, Graz University of Technology, Graz, Austria, and

Oszkar Biro
Institute of Fundamentals and Theory of Electrical Engineering, Graz University of Technology, Graz, Austria

Abstract

Purpose – This paper aims to introduce a non-invasive and convenient method to detect a life-threatening disease called aortic dissection. A Bayesian inference based on enhanced multi-sensors impedance cardiography (ICG) method has been applied to classify signals from healthy and sick patients.

Design/methodology/approach – A 3D numerical model consisting of simplified organ geometries is used to simulate the electrical impedance changes in the ICG-relevant domain of the human torso. The Bayesian probability theory is used for detecting an aortic dissection, which provides information about

COMPEL - The international journal for computation and mathematics in electrical and electronic engineering
Vol. 41 No. 3, 2022
pp. 824-839
Emerald Publishing Limited
0332-1649
DOI 10.1108/COMPEL-03-2021-0072

First and second authors contributed equally to this work.

the probabilities for both cases, a dissected and a healthy aorta. Thus, the reliability and the uncertainty of the disease identification are found by this method and may indicate further diagnostic clarification.

Findings – The Bayesian classification shows that the enhanced multi-sensors ICG is more reliable in detecting aortic dissection than conventional ICG. Bayesian probability theory allows a rigorous quantification of all uncertainties to draw reliable conclusions for the medical treatment of aortic dissection.

Originality/value – This paper presents a non-invasive and reliable method based on a numerical simulation that could be beneficial for the medical management of aortic dissection patients. With this method, clinicians would be able to monitor the patient's status and make better decisions in the treatment procedure of each patient.

Keywords Numerical analysis, Finite element method, Sensors, Impedance, Bioelectromagnetics, Uncertainties in electromagnetics, Bayesian inference, Probability theory, Impedance cardiography, Aortic dissection

Paper type Research paper

Nomenclature

$\boldsymbol{x}$ = Input parameters corresponding to $\boldsymbol{Z}$. The values of these parameters are unknown and must be inferred in the inverse problem;

$\boldsymbol{x}'$ = A measured set of values for input parameters corresponding to $\boldsymbol{Z}'$;

$\boldsymbol{Z}$ = ICG measurements for which the inverse problem should be solved based on the previously calibrated surrogate model. In this case, artificial data from the surrogate model, which is superimposed with random noise; and

$\boldsymbol{Z}'$ = ICG measurements used for calibration/training of the surrogate model. In this case, the FEM data.

1. Introduction

Aortic dissection (AD) is a hazardous aortic disease with high mortality. AD is commonly initiated by forming a tear in the intima, allowing blood to flow into the aortic wall. The fluid-dynamical forces separate the layers of the aortic wall, resulting in the formation of a true lumen and a false lumen (Figure 1) (Silaschi *et al.*, 2017). The false lumen represents the blood-filled space between the dissected layers of the aortic wall, whereas the true lumen is the usual passageway of blood. The symptoms of AD patients are sudden severe chest or upper back pain, which are not particularly assignable to this disease.

The feasibility of impedance cardiography (ICG) in the identification of AD has been investigated in Badeli *et al.* (2020), Reinbacher-Köstinger *et al.* (2019). Accordingly, it was concluded that monitoring the ICG signal could be an asset for detecting or tracking the disease's development, such as false lumen expansion.

Medical management of AD is based mainly on personal experience, expert opinion and historical observational studies as there is a paucity of randomized controlled studies. Clinicians very often have to make critical decisions with high uncertainties during the

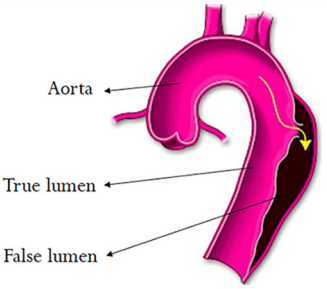

Figure 1.
Dissected Aorta (Silaschi *et al.*, 2017)

diagnosis of the patients. However, they try to reduce the uncertainty in clinical decisions and improve the patient's condition by using the available information obtained from various clinical and diagnostic tests, together with the patient's medical condition. The natural framework for quantifying uncertainties is the Bayesian probability theory. It is proven mathematically in Cox (1946), and in a more modern presentation in Sivia and Skilling (2006, App.B], that the Bayesian probability calculus is unique and thus, in fact, the only consistent and rigorous calculus to deal with uncertainties. Therefore, Bayesian probability theory could be applied to combine the results of multiple tests while treating AD. Thereby, in this paper, for detecting an AD, a Bayesian inference based on a proposed multi-sensors ICG method is performed in which the inverse problem is solved by Bayesian probability theory.

2. Simulation model

2.1 Sources of bioimpedance changes

The time-dependent transthoracic impedance $\underline{Z}(t)$ is composed of static thoracic base impedance $\underline{Z_0}$ and a time-dependent pulsatile impedance change $\Delta\underline{Z}(t)$. By eliminating the oscillating cardiac-asynchronous respiratory component, $\Delta\underline{Z}(t)$ is synchronous to cardiac activity. During the systolic phase of a cardiac cycle, the heart contracts to pump blood into the aorta, and in the diastolic phase, the heart relaxes after contraction. This pulsatile flow causes the volumetric expansion of the aorta and, in turn, a variation of blood conductivity inside the aorta (Badeli *et al.*, 2020; Reinbacher-Köstinger *et al.*, 2019). Another reason for blood conductivity changes is the orientation and deformation of the red blood cells (RBCs) in flowing blood. At higher velocities, the shear stress increases, which consequently deforms the RBCs in the layer with the highest stress close to the vessel wall and also aligns them throughout the vessel. Both effects lead to a higher conductivity compared to that of resting blood (σ_0) (Badeli *et al.*, 2020). Based on the formulations described in (Badeli *et al.*, 2020), the blood conductivity σ_{blood} has been defined as:

$$\sigma_{\text{blood}}\big(v(t), H\big) = \sigma_0(H) + \Delta\sigma_{\text{blood}}\big(v(t), H\big), \tag{1}$$

in which $v(t)$ and H represent the time-dependent blood velocity and the blood hematocrit level (the volume fraction of RBCs in the whole blood volume), respectively.

2.2 Finite element model

A 3D numerical simulation model has been set up in COMSOL Multiphysics for the underlying time-harmonic current flow problem. Since the cardiac cycle duration is much longer than the period of the injected current, simulations can be performed in the frequency domain. The electric potential drop is measured between the measuring sensors by solving Laplace's equation for the electric potential V:

$$\nabla \cdot ([\sigma + j\omega\varepsilon]\nabla V) = 0. \tag{2}$$

The model consists of a simplified geometry of the human thorax, as shown in Figure 2. A proposed multi-sensors configuration is used in which five pairs of source (injection) electrodes are placed on the surface of the thorax (each pair in one vertical line), which inject an alternating current with a magnitude of $5\,mA$ and a frequency of $100\,kHz$ asynchronously. For each injection, the electric potential drop is evaluated between five measurement sensor pairs (each pair in one vertical line) which leads to the thoracic impedance:

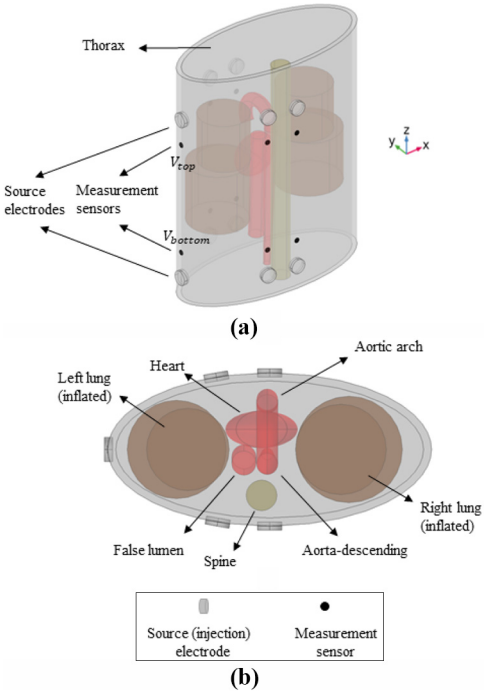

Note: (a) 3D view – (b) 2D bottomview

Figure 2
Simulation model setup

$$\underline{Z} = \frac{\underline{V}_{\text{top}} - \underline{V}_{\text{bottom}}}{\underline{I}}. \tag{3}$$

The boundary conditions are

- $V = const$ and $\int_S [\sigma + j\omega\varepsilon]\nabla V \cdot \boldsymbol{n} dS = I_0$, on the top source electrode;
- $V = 0$, on the bottom source electrode; and
- $\boldsymbol{n} \cdot [\sigma + j\omega\varepsilon]\nabla V = 0$, on the thorax surface.

where **n** is the normal unit vector. The blood conductivity in the aorta is changing according to (1) during the cardiac cycle. The electrical conductivity and permittivity of tissue types which are considered in the simulation model have been taken from data provided in Gabriel (1996). For other surrounding materials such as muscles, ribs and fat which are not considered directly in the simulation model, a mean conductivity and permittivity is assigned to the thorax domain to provide a realistic value for the static thoracic impedance $\underline{Z}_0$. To reduce the computational cost, only the first half of the cardiac cycle (0.5 *s*), which is the more significant phase, is considered.

Besides the fact that the false lumen changes the shape of the aorta, the blood flow is also disturbed and creates recirculation around the dissection. Flow disturbances inhibit the deformation and orientation of the RBCs; thus, the flow shear rate and, consequently, the blood flow induced conductivity changes will alter from that in a healthy case. These assumptions have been considered in the simulation model for different stages of AD in the same way as reported in Badeli *et al.* (2020).

The simulation model shown in Figure 2 will be used later to develop two surrogate models (for healthy and AD cases). For this purpose, different input parameters (to cover different physiological and pathological states) will be considered. These surrogate models will be used instead of the simulation model for further investigations.

3. Bayesian multi-sensors inference

3.1 Basic rules of probability theory

Probability is a measure of the truthfulness of a proposition (hypothesis). One has to distinguish between the probability $p(x)$ that a certain proposition x is true without further knowledge and the conditional probability $p(x|y)$ that the same proposition holds conditioned on some given information y, e.g. some measured data. Like in Boolean algebra, propositions can be combined by the logical AND ($\wedge$) and a logical OR ($\vee$). From hereon $p(x \wedge y)$ will be abbreviated by $p(x,y)$. Logically, for conditionally independent x and y, one finds $p(x,y) = p(x)p(y)$. By demanding a consistent logic only, the sum rule and the product rule are derived, see (Sivia and Skilling, 2006, Ch.1] (von der Linden *et al.*, 2014, Ch.1], or (Jaynes, 2003, Ch.1,2]. From them, one finds the marginalization rule and Bayes' theorem. For continuous variables, the marginalization rule takes an integral form:

$$p(x) = \int p(x|y)\ p(y)dy\,. \tag{4}$$

Bayes' theorem reads:

$$p(x|y) = \frac{p(y|x) \cdot p(x)}{p(y)}\,. \tag{5}$$

For example, x could be the model parameters and y the corresponding measured values. Then, $p(x)$ is the prior probability for the state of knowledge, or ignorance, about the parameters before the experiment. Detailed information for finding prior distributions is provided in Von Toussaint (2011). The likelihood $p(y|x)$ is the probability for the data y, given all parameters and the underlying physical model. In other words, by assuming certain model parameters, one should be able to determine the ideal values of the data f. Since experimental data always have noise, their measured value will be:

$$y = f + \varepsilon\,, \tag{6}$$

where ε is the experimental noise/uncertainty. The posterior $p(x|y)$ gives the probability that, by knowing the data, certain values of parameters describe the model. The denominator in equation (5) is the so-called evidence or the normalization.

3.2 Likelihood function and the surrogate model

In the inverse problem, one wants to infer the underlying model parameters, e.g. the false lumen radius, from the ICG measurements. Preliminarily, the parameters and the measurement data shall be denoted by x and y, respectively. Assuming that the model for the human body and its mathematical description, as far as ICG is concerned, is sufficiently realistic, then for specific model input-parameters x, the finite element (FEM) simulation yields values for the impedance $Z = f(x)$ that should deviate from the measured data y only due to the measurement noise, as discussed just before. Let us assume that the noise ε is

described by a density function $\rho(\varepsilon)$. Then the likelihood function, i.e. the probability density for the measured data, is given by $p(y|x) = \rho\big(f(x) - y\big)$ according to (6). The sought-for posterior probability for the model parameters, i.e. $p(x|y)$, is proportional to $\rho(f(x) - y)p(x)$. To plot the posterior or evaluate its characteristics, like mean and variance, $p(y|x)$ needs to be computed for a large number M of parameter values x. That implies that the FEM simulation has to be performed M-times to provide the true impedance value $f(x)$ in the likelihood. This will be very costly as far as CPU time is concerned. Therefore, it would be advantageous to have an easy to calculate surrogate model for the impedance to replace the complex FEM simulation.

Here two surrogate models, one for the healthy and one for the sick patient, will be developed. The simulation parameters for developing surrogate models have been chosen according to the sensitivity analysis study in the previous work (Badeli *et al.*, 2020). The surrogate model for the healthy case depends on only two patient variables, namely the maximum radius of the true lumen R_{TL} and the blood hematocrit level H. In the case of a sick patient, the surrogate model additionally depends on the radius of the false lumen R_{FL} and the angular position of the false lumen relative to the true lumen measured from the x-axis plane, α_{FL} (Figure 2). These parameters enter in Bayesian probability theory as random variables. For a detailed discussion on random variables, see (Sivia and Skilling, 2006, Ch.1] (von der Linden *et al.*, 2014, Ch.1], or (Jaynes, 2003, Ch.1,2]. The prior distributions for all variables have been assumed to be uniform within certain ranges since lack of knowledge does not allow specification of more informative priors. Table 1 includes the values for the prior ranges. Further, all four variables are logically independent of each other.

All variables $(R_{TL}, H, R_{FL}, \alpha_{FL})$ are subsumed in a vector $\boldsymbol{x} = (x_1, x_2, \cdots, x_{N_x})^T$, with $N_x = 2$ ($N_x = 4$) in the healthy (sick) case. Next, the time-dependent simulation outcome for the impedance $f(\boldsymbol{x}, t)$ shall be expanded in terms of time-independent basis functions $\phi_{\boldsymbol{p}}(\boldsymbol{x})$ by:

$$f(\boldsymbol{x}, t) = f\big(\boldsymbol{x}; \boldsymbol{c}(t)\big) = \sum_{\boldsymbol{p} \in P} c_{\boldsymbol{p}}(t)\, \phi_{\boldsymbol{p}}(\boldsymbol{x}). \tag{7}$$

In this work, a Polynomial Chaos Expansion (PCE) is used, e.g. (Crestaux *et al.*, 2009), where the basis functions $\phi_{\boldsymbol{p}}(\boldsymbol{x})$ are multi-variate polynomials that are orthogonal with respect to the L^2 inner product with probability measure $p(\boldsymbol{x})$. $\boldsymbol{c} = \{c_{\boldsymbol{p}}\}$ is a set of expansion coefficients and P is a set of multi-indices $\boldsymbol{p}$, denoting the expansion-order of each variable $x_1, x_2, \ldots x_{N_x}$ in the polynomial $\phi_{\boldsymbol{p}}(\boldsymbol{x})$. Next, FEM simulations are performed for a sufficient number of values for the input parameters. The input parameter values are indexed by m, $\boldsymbol{x}'(m)$, and gathered in the set $\boldsymbol{x}' = \{\boldsymbol{x}'(m)\}_{m=1}^{N_s}$ ($N_s = 300$) separately for the healthy and the sick condition. Then, the hyper-parameters $\boldsymbol{c}$ are inferred from the simulation data, i.e. $\boldsymbol{x}'$ and the corresponding simulation output values. Then, when new,

Cases	Variable	Distribution	Limits	Unit
Healthy	R_{TL}	Uniform	[1.35 1.95]	cm
Healthy	H	Uniform	[0.35 0.55]	1
Sick	R_{TL}	Uniform	[1.35 1.95]	cm
Sick	H	Uniform	[0.35 0.55]	1
Sick	R_{FL}	Uniform	[0.3 1.5]	cm
Sick	α_{FL}	Uniform	[2.9 3.65]	rad

Table 1. Specification of prior probabilities for the healthy and sick study cases

real impedance data from patients are available, the surrogate models can be used instead of the FEM simulations to determine the likelihood function and, subsequently, to calculate the posterior probability for the patient-specific parameters of interest $\boldsymbol{x}$.

In more detail, in the FEM simulation, 5 injection electrode pairs with labels $i = 1,\ldots,5$ and 5 sensor pairs with labels $j = 1,\ldots,5$ are located at positions that are best suited for inferring the sought-for patient parameters $\boldsymbol{x}$. The measurements are performed for a time series t_k ($k = 1,\ldots,N_t$) of half a cardiac cycle. For each of the N_s parameter sets $\boldsymbol{x}'(m)$, the resulting impedance data sets are $\{Z'_{ijk}{}^{(m)}\}$. One simulation for the healthy (H) and one for the sick (S) condition is performed. The FEM simulation has to be performed for each injection pair i separately to generate one corresponding time-series t_k with each sensor pair j. From these data, the parameters $\boldsymbol{c}$ for the two 4th-order surrogate model functions (PCE-cardinality $|P| = 4$) are determined as follows. It is assumed that the impedance-dependence on the patient-specific parameters $\boldsymbol{x}$ depends on the injection/sensor positions, as well as on the time within the cardiac cycle. Hence, the coefficients $\boldsymbol{c}$ depend on the indices i,j,k. The surrogate function for the impedance Z_{ijk} corresponding to injection/sensor pair indices i,j measured at time t_k is approximated by:

$$f(\boldsymbol{x};\boldsymbol{c}_{ijk}) = \sum_{\boldsymbol{p}\in P} \boldsymbol{c}_{\boldsymbol{p}}^{(ijk)} \Phi_{\boldsymbol{p}}(\boldsymbol{x})\,. \tag{8}$$

Next, the parameters $\boldsymbol{c}^{(ijk)}$ need to be estimated based on the FEM simulations described before. This is again an inverse problem that can be dealt with consistently in the frame of Bayesian probability theory. First, the simulation for one set of patient parameters $\boldsymbol{x}$ is considered. Bayes' theorem in (5) is invoked, where y now stands for the FEM data for the impedances $\boldsymbol{Z}' = \{Z'_{ijk}\}$, corresponding to specific input parameter values, and x stands now for the unknown coefficients $\boldsymbol{c} = \{\boldsymbol{c}_{ijk}\}$.

A simplification of the notation is achieved when a compound index l is introduced that enumerates the possible index sets $\{i,j,k\}$. Then, $\boldsymbol{Z}' = \{Z'_l\}$ and $\boldsymbol{c} = \{c_l\}$. The likelihood that covers the uncertainty of the data can be described by a Gaussian:

$$p\left(\boldsymbol{Z}'|\boldsymbol{c},\boldsymbol{x}\right) = \prod_l p\left(Z'_l|\boldsymbol{c}_l,\boldsymbol{x}\right), \tag{9}$$

with

$$p\left(Z'_l|\boldsymbol{c}_l,\boldsymbol{x}\right) = \frac{1}{\sqrt{2\pi\Delta_l^2}} \exp\left(-\frac{\left(Z'_l - f(\boldsymbol{x};\boldsymbol{c}_l)\right)^2}{2\Delta_l^2}\right). \tag{10}$$

The product form is due to the independence of the noises of the data. For the FEM-simulation, Δ_l stands for the numerical uncertainty, while later on Δ_l will be the sensor noise level. In both cases, the values of Δ_l are usually well known. For the sake of simpler notation, Δ will therefore not be written explicitly in the conditional complex of the probabilities. Likewise, the measurement times t_k will be suppressed in the conditional complex. In general, the noise may depend on the electrode configuration denoted by the index pair i,j. To determine the posterior probability for the sets of coefficients, we also need the prior $p(\boldsymbol{c})$. As there is no resilient prior knowledge, an uninformative constant prior can be used. In this case, the prior can be ignored altogether and

$$p\left(\boldsymbol{c}|\boldsymbol{Z}^{'},\boldsymbol{x}\right) \propto p\left(\boldsymbol{Z}^{'}|\boldsymbol{c},\boldsymbol{x}\right). \tag{11}$$

N_s such FEM data sets $\boldsymbol{Z}'(m)$ exist corresponding to the N_s training sets for the patient parameters $\boldsymbol{x}^{(m)}$. Along the previous line of reasoning with $D' = \{\boldsymbol{x}'(m), \boldsymbol{Z}'(m)\}_{m=1}^{N_s}$, i.e. $\boldsymbol{x}'$ instead of $\boldsymbol{x}$ in (11), we find:

$$p(\boldsymbol{c}|D') \propto \prod_{l,m} \exp\left(-\frac{\left(Z_l'(m) - f\left(\boldsymbol{x}'(m);\boldsymbol{c}_l\right)\right)^2}{2\Delta_l}\right). \tag{12}$$

There are two routes to proceed. In the first case, one assumes that the model description of the human body is correct and the FEM simulation, therefore, yields the impedance values that would be observable in a noise-free experiment. In that case, the only uncertainty stems from the numerical errors, which are very small. Due to the tiny noise level, the likelihood then turns into a Dirac-delta distribution, i.e:

$$p(\boldsymbol{c}|D') \to \prod_l \delta\left(\boldsymbol{c}_l - \hat{\boldsymbol{c}}_l\right), \tag{13}$$

with

$$\hat{\boldsymbol{c}}_l = \arg\max_{\boldsymbol{c}_l} p(\boldsymbol{c}|D'). \tag{14}$$

This delta-posterior probability leaves no room for uncertainties regarding the coefficients $\boldsymbol{c}$. In Appendix 1 it has been shown that the solution of equation (14) is given by

$$\hat{c}_{pl} = \sum_m \left(\left(M^T M\right)^{-1} M^T\right)_{pm} Z_l'(m) \qquad M_{mp} := \Phi_p\left(\boldsymbol{x}'(m)\right). \tag{15}$$

This is only valid if $M^T M$ is not singular. The second line of reasoning includes the uncertainty of the model description of the human body and the impedance calculation therein. In that case, the impedances obtained by FEM have additional uncertainties, which can also be described by the Gaussian in (10) and the noise level Δ_l has to be chosen appropriately.

3.3 Inverse problem

Now that the probability for the coefficients of the surrogate model $\boldsymbol{c}$, are determined from the training data $D^{'}$, the surrogate model can be used instead of the FEM simulations to infer the patient parameters $\boldsymbol{x}$ from newly measured impedance data $\boldsymbol{Z} = \{Z_l\}$ for which $\boldsymbol{x}$ is not known. I.e., one wants to compute the probability density for the parameters $\boldsymbol{x}$ that correspond to impedance measurements $\boldsymbol{Z}$, based on the previous data summarized by $D^{'}$, i.e. $p(\mathrm{x}|\mathrm{Z}, D')$. It is important to understand the difference in the meaning of $\boldsymbol{Z}'$, for which a corresponding set of values for the input parameters $\boldsymbol{x}'$ is known and used to determine the surrogate models' coefficients $\boldsymbol{c}$, and $\boldsymbol{Z}$ which will be introduced as independently measured set of ICG signals for which the corresponding set of values for the input parameters, $\boldsymbol{x}$, is not known and so must be inferred from $\boldsymbol{x}'$, $\boldsymbol{Z}'$ and $\boldsymbol{Z}$. To this end, first Bayes' theorem is invoked:

$$p(\mathrm{x}|\mathrm{Z}, D') = \frac{1}{\gamma} p(\mathrm{Z}|\mathrm{x}, D') p(\boldsymbol{x}|D') \,. \tag{16}$$

The normalization factor is independent of $\boldsymbol{x}$ and, therefore, unimportant here. The training data, D' does not contain information about the patient parameters $\boldsymbol{x}$ of the current patient to which the data $\boldsymbol{Z}$ belong. Therefore, the last factor is the bare prior $p(\boldsymbol{x})$ for the patient parameters. Next, the hyper-parameters $\boldsymbol{c}$ of the surrogate function via the marginalization rule can be introduced:

$$p(\mathrm{Z}|\mathrm{x}, D') = \int p(\mathrm{Z}|\mathrm{x}, D', \boldsymbol{c}) p(\mathrm{c}|\mathrm{x}, D') d\mathcal{V}_{\boldsymbol{c}} \,, \tag{17}$$

which is to be read as a volume integral over the domain of $\boldsymbol{c}$. In the second factor, the patient parameters $\boldsymbol{x}$ of the current patient without the corresponding impedance values do not contain any information about the hyper-parameters of the surrogate model, i.e. $p(\mathrm{c}|\mathrm{x}, D') = p(\boldsymbol{c}|D')$ is the posterior of the previous section. Finally, in the first term in the integral, the information D' is redundant, as $\boldsymbol{x}$ and $\boldsymbol{c}$ already contains the required information for the surrogate function entering the likelihood. Up to this point, the considerations are still quite general and allow the description of the inaccuracy in modelling the human body for the impedance calculation. In the remaining part of this paper, however, it is assumed that the modelling is exact and, consequently, the delta-distribution for the $p(\boldsymbol{c}|D')$ is as given in (13). Then the integral in equation (17) simplifies to:

$$p(\mathrm{Z}|\mathrm{x}, D') = p(\mathrm{Z}|\mathrm{x}, \hat{\boldsymbol{c}}) \,, \tag{18}$$

and in turn the sought-for posterior according to (16) becomes

$$p(\mathrm{x}|\mathrm{Z}, D') = \frac{1}{\gamma} p(\mathrm{Z}|\mathrm{x}, \hat{\boldsymbol{c}}) p(\boldsymbol{x}) \,. \tag{19}$$

From this quantity, one can infer parameter estimates, function estimates, associated uncertainties and model probabilities. The generalization to the case that the model description is not exact is in principle. In that case, however, the integral over the space of hyper-parameters $\boldsymbol{c}$ has to be evaluated numerically, e.g. by Monte-Carlo sampling. This concerns equation (17) and all integrals following in the next sections.

3.4 Parameter estimation and its uncertainty

The most probable values for the patient parameters $\boldsymbol{x}$, the so-called maximum a-posteriori (MAP) estimate, is the solution of the N_x-dimensional optimization problem $\hat{\boldsymbol{x}} = \mathrm{argmax}_{\boldsymbol{x}} p(\mathrm{x}|\mathrm{Z}, \hat{\boldsymbol{c}})$. However, there is little to be gained in finding the most probable $\boldsymbol{x}$ if it is not precisely pin-pointed to a single maximum such that one can neglect everything else. In most cases, this will not be fulfilled. However, this requirement indeed is fulfilled for the previous MAP approximation of the coefficients $\boldsymbol{c}$ of the PCE if it leads to the Dirac-delta distribution. A more reasonable quantity as parameter estimate is the expectation value along with the variance as a measure for the quadratic uncertainty. The parameter expectation values are given by:

$$\langle x_i^\nu \rangle = \int x_i^\nu \cdot p(\mathrm{x}|\mathrm{Z}, D') d\mathcal{V}_{\boldsymbol{x}} \approx \int x_i^\nu \cdot p(\mathrm{x}|\mathrm{Z}, \hat{\boldsymbol{c}}) d\mathcal{V}_{\boldsymbol{x}}. \tag{20}$$

The integral is to be understood as volume integral over the domain of $\boldsymbol{x}$, and the approximation in equation (13) has been used. According to Table 1, this defines a two-dimensional integral for model H (healthy patient model) and a four-dimensional integral for model S (sick patient model). The uncertainty of this estimate is as follows:

$$\Delta x_i = \sqrt{\langle x_i^2 \rangle - \langle x_i \rangle^2}. \tag{21}$$

3.5 Model comparison

Bayesian probability theory allows inferring whether or not a patient has an aortic dissection, based on impedance data $\boldsymbol{Z}$. To this end we use the probability $p(M|\boldsymbol{Z}, D')$ for $M \in \{H;S\}$. Bayes' theorem gives:

$$p(M|\boldsymbol{Z}, D') \propto p(\boldsymbol{Z}|D', M) p(M). \tag{22}$$

In the last term, the dependence on D' is omitted, as these data are irrelevant for the current patient; they only served to determine the hyper-parameters of the surrogate model. For a complete specification of the surrogate model, one needs to introduce the patient-specific unknown parameters $\boldsymbol{x}$ and hyper-parameters $\boldsymbol{c}$. Along with the delta-approximation in the equation (13) the marginalization over $\boldsymbol{c}$ simply replaces the information D' by $\hat{\boldsymbol{c}}$. The $\boldsymbol{x}$- marginalization then yields:

$$p(\boldsymbol{Z}|D', M) = \int p(\mathrm{Z}|\mathrm{x}, \hat{\boldsymbol{c}}, M) p(\boldsymbol{x}|M) d\mathcal{V}_{\boldsymbol{x}}. \tag{23}$$

As outlined earlier, a uniform prior has been used for the patient parameters within the certain parameter ranges $\boldsymbol{R}_M$, specified in Table 1, i.e.

$$p(\boldsymbol{x}|M) = \begin{cases} \dfrac{1}{\mathrm{Vol}(p(\boldsymbol{x}|M))} & \text{if } \boldsymbol{x} \in \boldsymbol{R}_M \\ 0 & \text{otherwise} \end{cases} \tag{24}$$

where $\mathrm{Vol}(p(\boldsymbol{x}|M))$ is the volume of the prior, i.e. the domain spanned by the (hyper-)cube specified in Table 1. Using the uniform prior, the integral becomes:

$$p(\boldsymbol{Z}|D', M) = \frac{1}{\mathrm{Vol}(p(\boldsymbol{x}|M))} \int_{\boldsymbol{R}_M} p(\mathrm{Z}|\mathrm{x}, \hat{\boldsymbol{c}}, M) d\mathcal{V}_{\boldsymbol{x}}. \tag{25}$$

The remaining integral can be considered as likelihood mass. A significant value means that the model describes the data well. Now the odds-ratio for the two models, which is the ratio of the two probabilities, can be calculated. Thereby, the unknown normalization in equation (22) drops out:

$$\frac{p(H|\boldsymbol{Z}, D')}{p(S|\boldsymbol{Z}, D')} = \frac{p(\boldsymbol{Z}|D', H)}{p(\boldsymbol{Z}|D', S)} \cdot \frac{p(H)}{p(S)}. \tag{26}$$

The first term on the r.h.s. is usually called Bayes factor and the second prior-odds. When substituting equation (25) into the Bayes factor, the appearing ratio $\mathrm{Vol}(p(\boldsymbol{x}|H))/\mathrm{Vol}(p(\boldsymbol{x}|S))$ is part of Ockham's razor and appears naturally. Ockham's razor avoids over-fitting and generally favours the less complex of two models. More details on Ockham's razor can be found in Sivia and Skilling (2006, Ch.4] (von der Linden *et al.*, 2014, Ch.3.3,17,27], or (Jaynes, 2003, Ch.8]. The other term that occurs is the ratio of the likelihood masses. This term favours the most flexible model, as it fits the data better. One can generally say that the simpler model wins if both models describe the data equally well. In contrast, the more complex model is more probable if it describes the data much better. In the following numerical analysis, both models are a priori chosen to be equally probable, i.e. the prior $p(M) = \frac{1}{2}$, and thus the prior odds ratio $p(H)/p(S)$ does not influence the outcome.

4. Results and discussion

The method is tested with artificial data. The integrals found in Sections 3-D to 3-E are analytically intractable and therefore solved numerically with the Markov Chain Monte Carlo method, particularly the Metropolis-Hastings algorithm (Brooks *et al.*, 2011, Ch.1] (von der Linden *et al.*, 2014, Ch.30.3],. The burn-in time was 10%, convergence and auto-correlations have been verified.

Figure 3 depicts the result of the Bayesian inference with the conventional tetra-polar spot electrode ICG (one pair of injection electrodes and one pair of measurement sensors) and the proposed multi-sensors ICG as described in Section 3. For this purpose, artificial data $\boldsymbol{Z}$ have been generated for a sick patient with specific patient parameters $(R_{TL} = 1.65cm, R_{FL} = 0.9cm, \alpha_{FL} = 3.275rad, H = 0.45)$, to which 4 different Gaussian

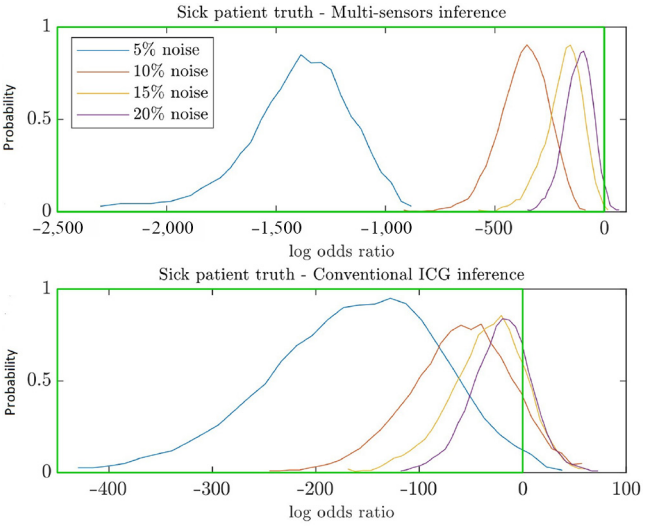

Figure 3.
Histogram of the logarithmic odds ratio for 1000 independent tests on a generated signal from a specific sick patient superimposed with 4 different noise levels with multi-sensors ICG inference (top) and conventional ICG inference (bottom)

Note: The probabilities have each been divided by their maximum value to facilitate easier comparison. This does not change the conclusions

noise levels have been added. Then, the logarithm of the odds-ratio (24) has been computed. This has been repeated 1000 times for each noise level independently. Due to the definition of the odds-ratio (26), negative values of the logarithmic odds-ratio correspond to a correct classification because the data are generated for a sick patient. The green lines in Figure 3 have denoted this. It is clear that the results from multi-sensors inference are more decisive compared to the conventional method. In particular, the multi-sensors inference is more robust to higher noise levels.

Figure 4 shows a comparison between the reliability of the conventional ICG method and multi-sensors ICG in detecting the source of a random noisy signal. For this purpose, 100 tests were performed for each noise level. In more detail, true patient parameters $\boldsymbol{x}$ have been chosen randomly, and a data set is generated according to the surrogate model and superimposed with noise. This is repeated 50 times for the healthy patient and 50 times for the sick patient (according to the chosen prior-odds). It is evident that the proposed Bayesian classification of multi-sensors ICG is more reliable than that of conventional type, although the uncertainty of the classification increases at higher noise levels. In practice, the prior-odds is not 1 but given by the ratio of the number of healthy people to the number of people with AD in the population (gender, age, acute symptoms, etc.) under consideration. A typical value for aortic dissection would be 10^5 based on its one-year incidence, meaning that the histogram in Figure 3 would be shifted to the right by 5 on the logarithmic scale of the odds ratio. Given that the distributions here span over a much larger scale of hundreds or thousands in the log odds ratio, this shift is negligible. It also means that the Bayes factor (the data term) here outweighs the prior odds by far. Nevertheless, it increases slightly the number of false negatives as well as false positives in Figure 4.

Figure 5 shows a Bayesian parameter estimation based on multi-sensors ICG data of a sick patient, with specific patient parameters, as mentioned before, for 4 different noise levels. It is obvious that, at higher noise levels, the estimated values for the most sensitive parameters shaping the ICG signal (Badeli *et al.*, 2020), such as the radius of the true lumen (R_{TL}) and the radius of the false lumen (R_{FL}), slightly differ from the true values. However, they are still within the statistical uncertainty.

Finally, the relationship of this work with Ranftl *et al.* (2019; Ranftl *et al.* (2019) will be discussed. The physical model used in the mentioned paper is somehow similar, however in this work, apart from the aorta, the surrounding tissues with their actual material properties have been modelled in the simulation domain. Also,

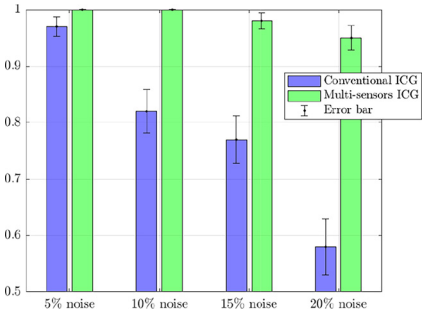

Figure 4.
Comparison between the reliability of the conventional ICG (blue) and multi-sensors ICG (green) to classify the source of 100 randomly generated noisy signals either from sick or healthy patients

interdependence between the blood conductivity changes in the true lumen and the size of the false lumen has been considered, as in Badeli *et al.* (2020). Furthermore, in Ranftl *et al.* (2019) and Ranftl *et al.* (2019), a tetra-polar spot electrode configuration (one pair of injectors and one pair of sensors) for measuring the impedance is used while in this work, multiple injectors and multiple sensors have been placed on the thorax's surface which shows a significant improvement for the diagnosis purposes (Ranftl *et al.*, 2019; Ranftl *et al.*, 2019). focuses on the methodology of surrogate modelling and forward propagation of uncertainty, while this work concerns the inverse problem, particularly the model selection and parameter estimation (Ranftl *et al.*, 2019; Ranftl *et al.*, 2019). uses multi-fidelity data, while this work uses multi-sensor data, with the essential difference being that the sources cannot *a priori* be ordered according to their fidelity. Note that here Polynomial Chaos Expansions are used as surrogate model, while (Ranftl *et al.*, 2019) uses a simple linear regression model and (Ranftl *et al.*, 2019) a generalized auto-regressive sequence of Gaussian processes.

5. Conclusion

A 3D numerical simulation model is developed in this work to detect aortic dissection in a human body. Also, it has been investigated whether the multi-sensors ICG data is advantageous. Bayesian probability theory is invoked to estimate the patient parameters entering the simulation model and for the classification of whether or not a patient suffers from AD. The approach is benchmarked based on artificial data for different noise levels of the sensors. The Bayesian classification/model comparisons show that the proposed multi-sensors ICG is more reliable than conventional tetra-polar spot electrode ICG. In addition, the values of the patient parameters are determined, which revealed that, in particular, the sizes of the true and false lumen can be reconstructed surprisingly accurately from the ICG data. All in all, Bayesian probability theory allows a rigorous quantification of all uncertainties in order to draw reliable conclusions for the medical treatment of aortic dissection.

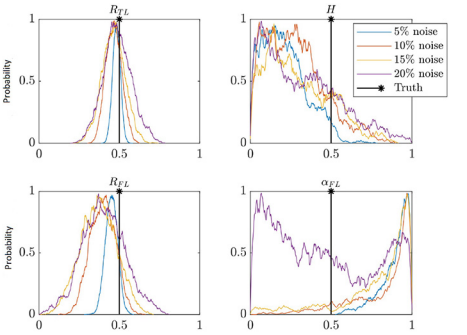

Note: In this plot, the parameter values are normalized between 0 and 1. The probabilities each been divided by their maximumvalue to facilitate easier comparison. This does not change the conclusions

Figure 5.
Parameter estimation by applying multi-sensors Bayesian inference on a generated signal from a specific sick patient superimposed with with 4 different noise levels

For future works, clinical trials will be done in cooperation with industrial and clinical partners in order to verify the proposed multi-sensors approach for detecting AD. Also, the uncertainties of the surrogate model and noise terms will be included in the Bayesian inference. Furthermore, the model will be extended to consider thrombosis in the false lumen and its impact on the impedance cardiogram.

References

Badeli, V., Melito, G.M., Reinbacher-Köstinger, A., Bíró, O. and Ellermann, K. (2020), "Electrode positioning to investigate the changes of the thoracic bioimpedance caused by aortic dissection – a simulation study", *Journal of Electrical Bioimpedance*, Vol. 11 No. 1, pp. 38-48.

Brooks, S., Gelman, A., Jones, G. and Meng, X.-L. (2011), *Handbook of Markov Chain Monte Carlo*, Chapman and Hall - CRC.

Cox, R.T. (1946), "Probability, frequency and reasonable expectation", *American Journal of Physics*, Vol. 14 No. 1.

Crestaux, T., Le Maître, O.P. and Martinez, J. (2009), "Polynomial chaos expansion for sensitivity analysis", *Reliability Engineering and System Safety*, Vol. 94 No. 7, pp. 1161-1172.

Gabriel, S. (1996), "The dielectric properties of biological tissues ", *Physics in Medicine and Biology*, Vol. 41 No. 11, pp. 2231-2249.

Jaynes, E.T. (2003), *Probability Theory: The Logic of Science*, Cambridge University Press.

Ranftl, S., Melito, G.M., Badeli, V., Reinbacher-Köstinger, A., Ellermann, K. and von der Linden, W. (2019), "On the diagnosis of aortic dissection with impedance cardiography: a Bayesian feasibility study framework with multi-fidelity simulation data", *Proceedings*, Vol. 33 No. 1, p. 24.

Ranftl, S., Melito, G.M., Badeli, V., Reinbacher-Köstinger, A., Ellermann, K. and von der Linden, W. (2019), "Bayesian uncertainty quantification with multi-fidelity data and gaussian processes for impedance cardiography of aortic dissection", *Entropy*, Vol. 22 No. 1, p. 58.

Reinbacher-Köstinger, A., Badeli, V., Bíró, O. and Magele, C. (2019), "Numerical simulation of conductivity changes in the human thorax caused by aortic dissection", *IEEE Transactions on Magnetics*, Vol. 55 No. 6.

Silaschi, M., Byrne, J. and Wendler, O. (2017), "Aortic dissection: medical, interventional and surgical management", *Heart*, Vol. 103 No. 1, pp. 78-87.

Sivia, D. and Skilling, J. (2006), *Data Analysis: A Bayesian Tutorial*, Oxford Univerity Press.

von der Linden, W., Dose, V. and von Toussaint, U. (2014), *Bayesian Probability Theory: Applications in the Physical Sciences*, Cambridge University Press.

Von Toussaint, U. (2011), "Bayesian inference in physics", *Reviews of Modern Physics*, Vol. 83 No. 3, pp. 943-999.

Appendix 1

Maximization of the likelihood concerning $\boldsymbol{c}$ in (14), in order to determine $\boldsymbol{c}$, is equivalent to minimization of the exponent of the product in (12). For this exponent χ, we find

$$\chi = \sum_{ml} \frac{1}{\Delta_l^2} \left(Z_l^{(m)} - \sum_p \underbrace{\Phi_p(\boldsymbol{x}^{(m)})}_{:=M_{mp}} c_{pl} \right)^2$$

$$= \sum_{ml} \frac{1}{\Delta_l^2} \left(\left(Z_l^{(m)} \right)^2 - 2 Z_l^{(m)} \textstyle\sum_p M_{mp} c_{pl} + [\sum_p M_{mp} c_{pl}] 2 \right).$$

The derivative wrt $c_{p'l'}$ yields

$$\frac{\partial \chi}{\partial c_{p'l'}} = -2 \frac{1}{\Delta_{l'}^2} \sum_m Z_{l'}^{(m)} M_{mp'} + 2 \frac{1}{\Delta_{l'}^2} \sum_m \left[\sum_p M_{mp} c_{pl} \right] M_{mp'}.$$

The condition for the minimum reads

$$\begin{aligned} \sum_m M_{mp'} Z_{l'}^{(m)} &= \sum_m \left[\sum_p M_{mp} c_{pl} \right] M_{mp'} \\ &= \sum_p \left[\sum_m M_{mp'} M_{mp} \right] c_{pl} \\ &= \sum_p (M^T M)_{p'p} c_{pl} \end{aligned}$$

If the inverse of MTM exists, the solution is (15).

Appendix 2

Signal Estimation and its Uncertainty

As a by-product, one finds the estimate for the reconstructed true (de-noised) signal and its uncertainty. For simplicity, the subscript $l = (i,j,k)$ is dropped here. Then the ν-th moments are

$$\begin{aligned} \langle f^\nu \rangle &= \int f^\nu p\left(f|D,D'\right) d\mathcal{V}_f \\ &= \int f^\nu p(f|\boldsymbol{x},\boldsymbol{c}) p\left(\boldsymbol{x}|D,D'\right) d\mathcal{V}_f d\mathcal{V}_{\boldsymbol{x}} \\ &\approx \int \left(f(\boldsymbol{x},\hat{\boldsymbol{c}}) \right)^\nu p\left(\boldsymbol{x}|\hat{\boldsymbol{c}},D'\right) d\mathcal{V}_{\boldsymbol{x}} \end{aligned} \tag{27}$$

where it has been used in the second line that, given input $\boldsymbol{x}$ and $\hat{\boldsymbol{c}}$, the function value f is determined, i.e. there is a Dirac-delta in f. The signal estimate and its uncertainty are then given by $\nu = 1,2$ and $\Delta f = \sqrt{\langle f^2 \rangle - \langle f \rangle^2}$. Note that the approximation in (13) has been used analogous to (20). Figure A1 shows the reconstructed signal from the case described in Section III-D. The reconstructed signal conforms with the true signal even for higher noise levels. It is worth mentioning that the uncertainty band gets wider by increasing the noise levels, but since the uncertainty band is in a much smaller

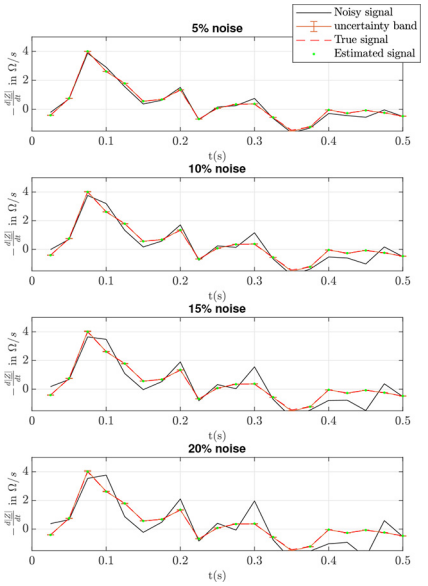

Figure A1.
Signal estimation with Bayesian multi-sensors inference on a signal from a specific sick patient superimposed with 4 different noise levels

range (10^{-3}) than the signal, it is not visible in Figure A1 and does not have a noticeable effect on the reconstructed signal. The correct signal reconstruction underlines the validity of our model and may improve estimates of, e.g. the stroke volume.

Corresponding author
Vahid Badeli can be contacted at: vahid.badeli@tugraz.at